Scanning transmission X-ray microscopy study of microbial calcification

K. BENZERARA,[1] T. H. YOON,[1] T. TYLISZCZAK,[2] B. CONSTANTZ,[3] A. M. SPORMANN[4] AND G. E. BROWN, JR[1,5]

[1]*Surface and Aqueous Geochemistry Group, Department of Geological and Environmental Sciences, Stanford University, Stanford, CA 94305-2115, USA*
[2]*Lawrence Berkeley National Laboratory, Advanced Light Source, Berkeley, CA 94720, USA*
[3]*Skeletal Kinetics, 10201 Bubb Road, Cupertino, CA 95014, USA*
[4]*Departments of Civil & Environmental Engineering, of Biological Sciences, and of Geological & Environmental Sciences, Stanford University, Stanford, CA 94305, USA*
[5]*Stanford Synchrotron Radiation Laboratory, SLAC, 2575 Sand Hill Road, Menlo Park, CA 94025, USA*

ABSTRACT

Calcium phosphates and calcium carbonates are among the most prevalent minerals involved in microbial fossilization. Characterization of both the organic and mineral components in biomineralized samples is, however, usually difficult at the appropriate spatial resolution (i.e. at the submicrometer scale). Scanning transmission X-ray microscopy (STXM) was used to measure C K-edge, P L-edge, and Ca L-edge near-edge X-ray absorption fine structure (NEXAFS) spectra of some calcium-containing minerals common in biomineralization processes and to study the experimental biomineralization by the model microorganism, *Caulobacter crescentus*. We show that the Ca $L_{2,3}$-edges for hydroxyapatite, calcite, vaterite, and aragonite are unique and can be used as probes to detect these different mineral phases. Using these results, we showed that *C. crescentus* cells, when cultured in the presence of high calcium concentration, precipitated carbonate hydroxyapatite. In parallel, we detected proteins, polysaccharides, and nucleic acids in the mineralizing bacteria at the single-cell scale. Finally, we discussed the utility of STXM for the study of natural fossilized microbial systems.

Corresponding author: K. Benzerara, tel.: 1 650 723 4782; fax: 1 650 725 2199; e-mail: benzerar@stanford.edu

INTRODUCTION

Microbes are often associated with calcium-containing minerals in nature, but it is usually difficult to determine if these organisms are involved in mineral nucleation. Finding biosignatures in minerals has been the goal of many recent studies to detect microbial remnants in the fossil record (e.g. Mojzsis & Arrhenius, 1998; Blake *et al.*, 2001; Sanchez-Navas & Martin-Algarra 2001). The same need arises in medical sciences where identification of the organics mixed with minerals would help in understanding the origin of some diseases (e.g. Dorozhkin & Epple, 2002; Ghidoni, 2004; Trion & Van der Laarse, 2004). One example showing the similarity of issues in geobiology and medical science is the debated existence of nanobacteria. Many studies have proposed that very small microorganisms called nanobacteria, which are smaller than the theoretical size limit for an autonomous viable organism (Nealson, 1999), are involved in the formation of calculi (e.g. Kajander *et al.*, 2003; Miller *et al.*, 2004). Nanobacteria are also thought to have a potential role in carbonate and phosphate precipitation in natural systems, according to some studies (Folk, 1999). Some authors have argued that these conclusions, which are usually based on morphological observations, are incorrect, and they have shown convincingly that precipitation of calcium phosphates on simple macromolecules can lead to the formation of similar complex organo-mineral patterns with bacterial-like morphologies (Vali *et al.*, 2001).

The problem of distinguishing between these two possibilities is in part methodological, as one needs to characterize both the mineral and the organic content of these submicrometer-sized objects. Transmission electron microscopy is a unique technique for characterizing crystallized minerals at the required spatial scale. However, characterization of organic

molecules present in a nanometer-sized object is much more difficult. Here, we show how scanning transmission X-ray microscopy (STXM) can be used to obtain high spatial and energy resolution near-edge X-ray absorption fine structure (NEXAFS) spectra at the C K-edge and the Ca $L_{2,3}$-edge on both the minerals and associated organics during biomineralization by *Caulobacter crescentus* cells under laboratory conditions. This work builds on our recent STXM study of microenvironments associated with a fossilized microorganism involved in pyroxene weathering (Benzerara *et al.*, 2005).

EXPERIMENTAL METHODS

Reference compound preparation

Calcite and aragonite powders were prepared from natural samples obtained from the Stanford University Research Mineral Collection (CA, USA). Vaterite powders were synthesized according to the method of Kralj *et al.* (1994). The same samples were previously used by Doyle *et al.* (2004) in a study of the effect of carbonate coatings on magnetite surfaces on chromate reduction. Powdered samples of abiotically synthesized hydroxyapatite were obtained from Riedel-de Haen (Germany). The phase purity of the powders was checked by X-ray diffraction (XRD) and the powders were found to be monomineralic. These powders were suspended for a few seconds in Milli-Q grade water, and one drop was deposited on the membrane of a holey carbon-coated 200 mesh copper grid and dried in air.

Bacterial cultures

The *Caulobacter crescentus* CB15 strain was kindly provided by P. I. Entcheva and A. Spormann (Stanford University). *C. crescentus* is a Gram-negative α-proteobacterium found in many oligotrophic natural environments (see Poindexter, 1981 for a review of the natural distribution of *Caulobacter* species). *Caulobacter* sp. is also found in many sewage treatment waters rich in phosphate (Macrae & Smit, 1991). This bacterium was considered a useful model for a biomineralization and bioremediation study because its genome has been recently sequenced (Nierman *et al.*, 2001) and extensive banks of mutants already exist, which offers the possibility of better understanding the biochemical processes involved in microbial calcification in the near future. Moreover, several studies are in progress to understand the resistance mechanisms of this microorganism to the toxicity of metals, in which, metal phosphate precipitation may potentially be one of these mechanisms (e.g. Levinson *et al.*, 1996).

C. crescentus cells were cultured in peptone yeast extract medium (PYE), which is referred to here as 'regular medium' and consists of bactotryptone (2 g L^{-1}), yeast extract (1 g L^{-1}), $MgSO_4$ (1 mM), and $CaCl_2$ (0.5 mM). The calcification medium was designed by adding $CaCl_2$ to PYE to a final concentration of 8 mM. Control tubes consisted of (a) the calcification medium, prior to inoculation, where no carbonate or phosphate precipitation was detected, and (b) the inoculated regular PYE growth medium. Two replicates of the three different samples were incubated under the same conditions at 30 °C during 20 days with continual shaking (200 r.p.m). Additional *C. crescentus* cultures in the regular PYE growth medium were incubated for only 2 days. After culturing, liquid suspension were centrifuged and washed with a sterile ionic strength buffer (0.01 M $NaNO_3$, pH = 7). One drop of each solution was deposited on a Si_3N_4 STXM sample holder and dried in air.

STXM observations and data analyses

STXM studies were performed at advanced light source (ALS) branch line 11.0.2.2 (Tyliszczak *et al.*, 2004) with the synchrotron storage ring operating at 1.9 GeV and 200–400 mA stored current. A 150 L mm^{-1} grating and 20 μm exit slit were used for carbon K-edge imaging and spectroscopy, providing a theoretical energy resolution of 100 meV. A 1200 L mm^{-1} grating and 30 μm slit were used for calcium $L_{2,3}$-edge measurements, providing a theoretical resolution of around 70 meV. Energy calibration was accomplished using the well-resolved 3p Rydberg peak at 294.96 eV of gaseous CO_2 for the C K-edge and the L_3 NEXAFS peak in the calcite Ca L-edge NEXAFS spectrum, which occurs at 349.3 eV (Rieger *et al.*, 1986).

STXM is a transmission microscopy using a monochromated X-ray beam produced by synchrotron radiation. Recent applications to colloids are presented in Yoon *et al.* (2004). The energy of the beam can be varied by less than 0.1 eV increments over a wide energy range (130–2100 eV). The beam is focused on the sample using a condenser zone plate and a 2-D image is collected by scanning the sample stage at a fixed photon energy. The image contrast results from differential absorption of X-rays depend on the chemical composition of the sample. Image stacks or line scans of reference Ca-carbonate and Ca-phosphate minerals and bacteria-mineral mixtures were used to collect C K-edge and Ca $L_{2,3}$-edge NEXAFS spectra. Image stacks or line scans were taken by scanning the sample in the x-y direction (image stack) or x direction (line scan) of selected sample areas at energy increments of 0.1 eV over the energy range of interest (280–305 eV for carbon, 342–360 eV for calcium). Here, x refers to the horizontal direction, y to the vertical direction, and the x-y plane to the plane perpendicular to the X-ray beam direction. The stack image procedure thus consists of measuring the NEXAFS spectrum for a specific element on each pixel (one pixel can be as small as 30 nm) of the image. Counting times are of the order of few milliseconds or less per pixel. Normalization and background correction of the Ca $L_{2,3}$-edge and C K-edge NEXAFS spectra were performed by dividing each spectrum by a second spectrum from a Ca- or C-free location on the same sample. Maps of calcium and phosphorus distributions were obtained by subtracting the image below the Ca or P $L_{2,3}$-edge, respectively, from the image of the same area above
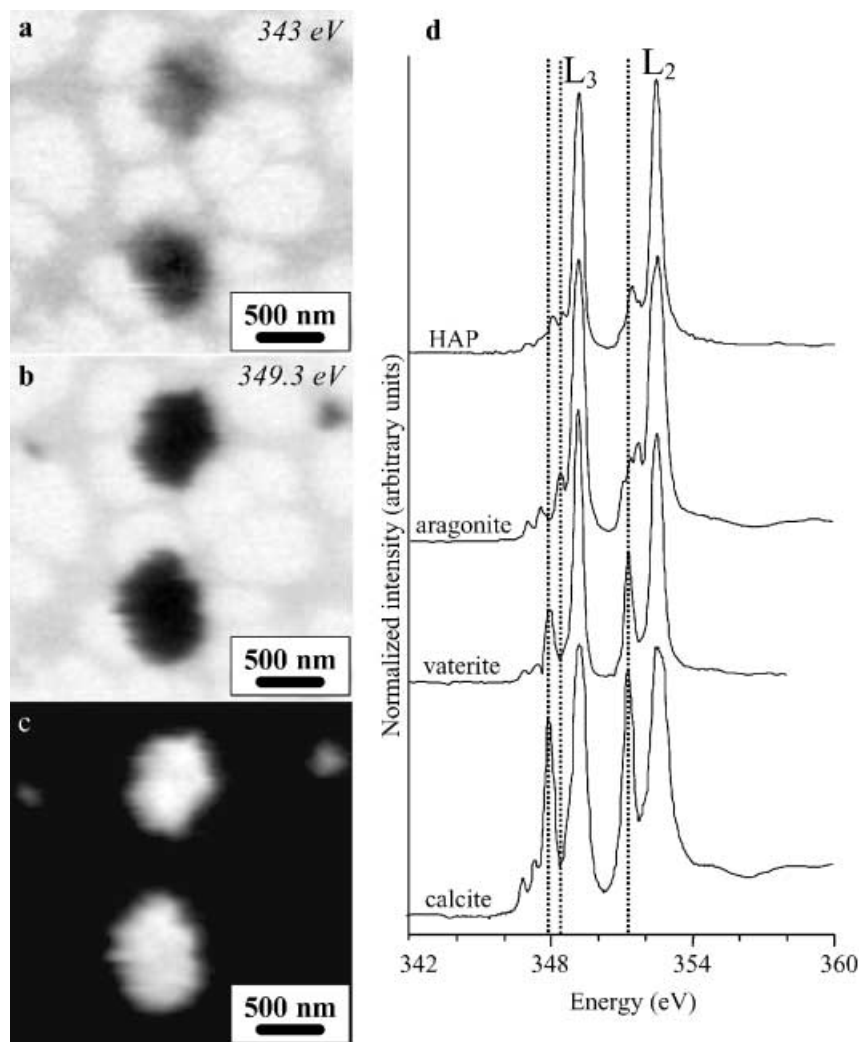
Fig. 1 Spectromicroscopy on calcium-containing reference compounds. (A) STXM image of hydroxyapatite particles at 343 eV (below the Ca $L_{2,3}$-edge). (B) STXM image of the same area at 349.3 eV (i.e. at the L_3 resonance energy). Particles appear much darker, showing the presence of calcium. (C) Calcium map obtained by subtraction of (A) and (B) converted into optical density (OD) units. (D) Calcium $L_{2,3}$-edge NEXAFS spectra of hydroxyapatite (HAP), aragonite, vaterite, and calcite. Vertical dotted lines show correlations between HAP and aragonite as well as between calcite and vaterite.

the edge. AXIS 2000 software (version 2 1n) (Hitchcock, 2000) was used to align image stacks and extract NEXAFS spectra from image stack or line scan measurements.

RESULTS

Ca $L_{2,3}$ edge NEXAFS of reference compounds

Figure 1 shows the image of reference hydroxyapatite particles at different energies as well as the Ca $L_{2,3}$-edge NEXAFS spectra of hydroxyapatite and the three most common calcium carbonate polymorphs in biomineralized systems (i.e. calcite, aragonite and vaterite). Each STXM image was taken at a single energy and provides a spatial resolution of approximately 25 nanometers. Two images were taken, respectively, at an energy below the Ca $L_{2,3}$-edge (approximately 347 eV) and above the edge (Figs 1A,B). By subtracting both images converted into optical density (OD) units, it is possible to obtain a calcium distribution map (Fig. 1C). This energy-filtered imaging procedure is an interesting first step in locating specific

element of interest in a heterogeneous mixture of particles. Moreover, a semiquantitative estimate of calcium content can be obtained, as the intensity of each pixel is directly related to the mass of calcium present in the pixel volume by the relation:

$$\Delta(O \cdot D)_X = \mu_X \cdot \rho \cdot d$$

where μ is the X-ray mass absorption coefficient for calcium at the energy X, ρ is the density in g m^{-3}, and d the thickness of the sample (in m). It is moreover possible to measure the Ca $L_{2,3}$-edge NEXAFS spectrum for the same area. Spectra were recorded on several particles for each mineral phase. Particles selected for NEXAFS measurements had an approximate size of 500 nm and absorbed approximately 60% of the incident beam at 350 eV. The energy position of the L_3-edge main peak of calcite was arbitrarily fixed at 349.3 eV, following Rieger et al. (1986), and the Ca $L_{2,3}$ edge of calcite was used as an energy calibration standard. The Ca $L_{2,3}$-edge spectrum shows two well resolved features (Fig. 1D) corresponding to the L_3

Table 1 Names, formulae, Ca-coordination numbers, and major XANES peak positions of Ca-containing minerals used in this study

Mineral name (source)	Formula	Ca-coordination number	Ca K-edge XANES peak positions (eV)
Hydroxyapatite	$Ca_{10}(PO4)_6(OH)_2$	8.4	347.1, 347.7, 348.2, 348.6, 349.3, 351.6 (351.8), 352.5
Vaterite	$CaCO_3$	6	347, 347.5, 348.1, 349.3, 351.4, 352.6
Calcite	$CaCO_3$	6	346.9, 347.4, 348, 349.3, 351.4, 352.6
Aragonite	$CaCO_3$	9	347.2, 347.7, 348.5, 349.3, 351.2, 351.5, 351.8, 352.6
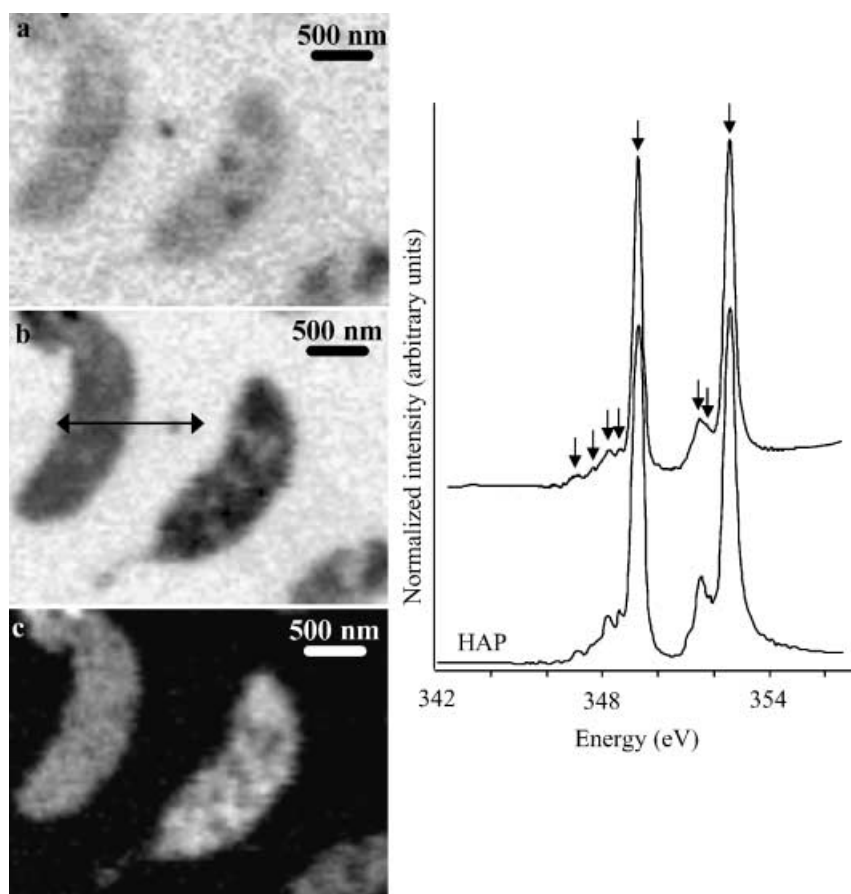
Fig. 2 Spectromicroscopy on *Caulobacter crescentus* incubated for 3 weeks in calcium rich (8 mM) growth medium at the calcium $L_{2,3}$-edge. (A) STXM image of *C. crescentus* cells at 343 eV (below the Ca $L_{2,3}$ edge). (B) STXM image of the same area at 349.3 eV showing the kidney bean shaped cells. The arrow shows the location where the line scan was processed, i.e. the trace of the analysis spots. Half of the spots are inside the bacterium, the other half are on the carbon-film providing I0. (C) Calcium map (generated by subtracting Fig. 2 (A) from Fig. 2 (B)) showing the calcium enrichment of cells with small variations in intensity between the two cells observed related to slight differences in calcium enrichment. (D) Calcium $L_{2,3}$-edge NEXAFS spectra of a *C. crescentus* cell shown in B. The spectra were identical for all the areas tested. Peak positions were 347.1, 347.7, 348.2, 348.6, 349.3, 351.5, and 352.6. A reference hydroxyapatite calcium $L_{2,3}$-edge NEXAFS spectrum is shown for comparison and displays the same peaks (see arrows).

(349.3 eV) and L_2 (~352.6 eV) edges of Ca. These main edge features do not show much variation in energy position among the different minerals examined here. However, the number, position, and intensity of other smaller peaks are specific to the different mineral phases and can be used to distinguish among them. The energy positions of all the peaks as well as the coordination numbers of calcium in the different mineral standards are given in Table 1.

STXM study of biomineralization by *Caulobacter crescentus*

Figure 2 shows *Caulobacter crescentus* cells incubated for 3 weeks in the calcification medium. *C. crescentus* cells are kidney bean-shaped of dimensions 2 µm long and 0.7 µm wide. A polar appendage, known as a stalk, was observed on some cells. The calcium map shows that calcium is distributed throughout the cells (Fig. 2C). The calcium concentration is estimated to be 10^{-14} g µm^{-2} in the cells depicted in Fig. 2 and is up to 10^{-13} g µm^{-2} in more biomineralized cells. Taking in account the counting time used for these measurements, the detection limit of Ca was estimated to be about 10^{-18} g µm^{-2}. Ca $L_{2,3}$-edge NEXAFS spectra were acquired on the cells using line scans. This procedure is preferred to measuring the absorption at a single point inside the cells as it reduces the exposure time at each point and hence, the extent of beam damage. Despite these precautions, some beam damage still occurred occasionally, as seen in Fig. 3.

The calcium $L_{2,3}$-edge NEXAFS spectra measured for different cells and at different locations within a single cell were identical and characteristic of hydroxyapatite (Fig. 2).

Figure 3 shows the distribution map of phosphorus in the same area as that depicted in Fig. 2. P L_3-edge NEXAFS spectra were very noisy and are not shown. Phosphorus was detected in the cells grown in the calcification medium and
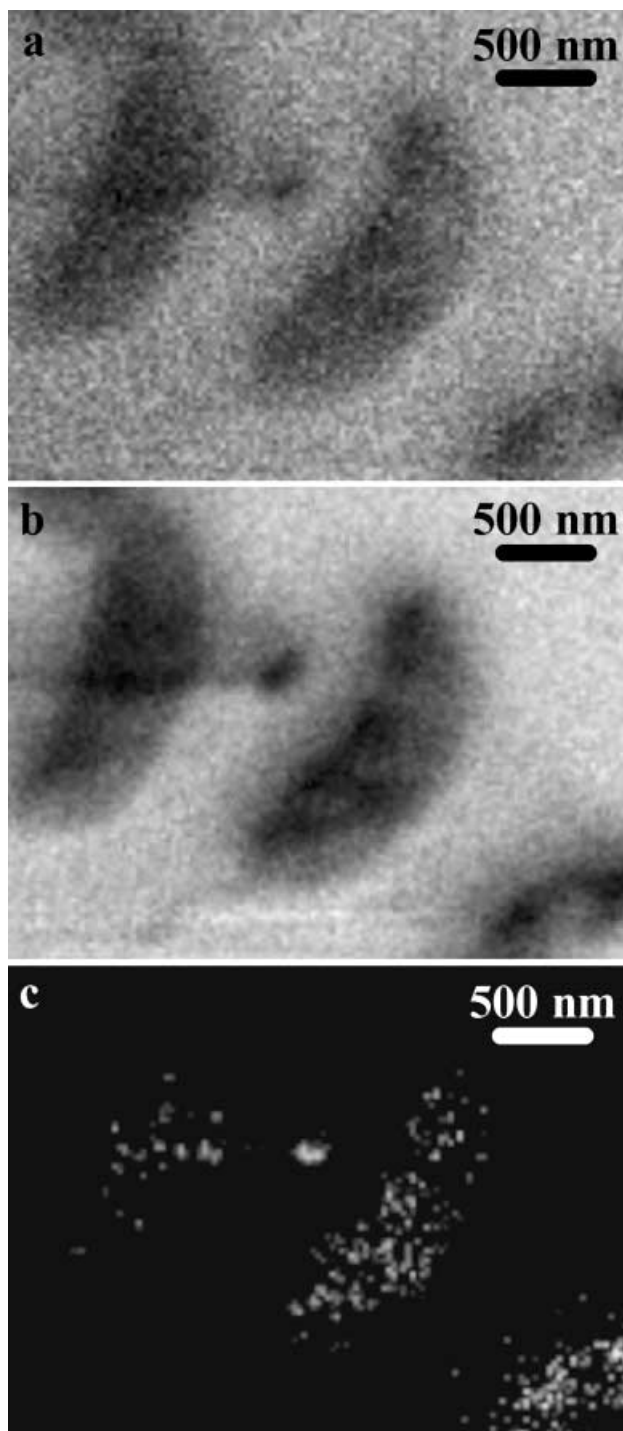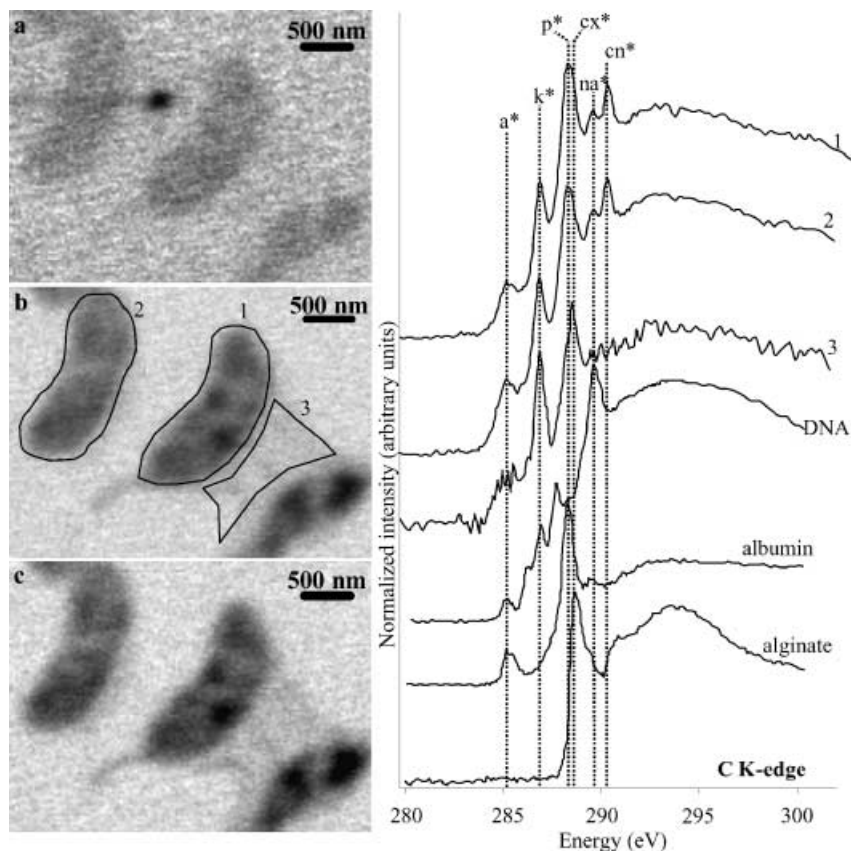
Fig. 3 STXM images of *C. crescentus* cells shown in Fig. 2 at the phosphorus L$_{2,3}$-edge. (A) STXM image below the P L$_{2,3}$-edge at 130 eV. (B) Image at 145 eV, which is above the P L$_{2,3}$ edge. The dark line across the cell on the left hand side is the result of beam damage resulting from the line scan at the Ca L$_{2,3}$-edge (see Fig. 2A). (C) Phosphorus map (generated by subtracting image 3a from image 3B) showing phosphorus enrichment of the cells. No phosphorus was detected using the same counting time on cells cultured in regular PYE medium. Rough estimation of the elemental concentration can be obtained from this image. The concentration of phosphorus is of the same magnitude as that of calcium.

its concentration was estimated to be of the same order of magnitude as that of calcium (i.e. 10^{-14} g µm^{-2}). More precise estimation of the Ca/P ratio was not possible. Phosphorus is an important elemental constituent of cellular nucleic acids and phospholipids; however, neither phosphorus nor calcium was detected in *C. crescentus* cells cultured in the regular PYE growth medium using the same counting time (data not shown). This suggests that the phosphorus and calcium concentrations were much lower in the cells under these conditions.

The carbon content of the mineralized cells was also characterized. Figure 4 shows C K-edge images of the same area studied at the Ca and P L$_{2,3}$-edges (see Figs 2 and 3) taken at an energy below the C K-edge (280 eV) (Fig. 4A) and at two different energies above the C-K edge (288.2 eV and 288.5 eV). Spectra were measured using the image stack procedure. The acquisition time at each energy step was 0.4 ms per pixel, which greatly reduces beam damage. Any area of interest in the image can then be chosen during data processing to obtain a C K-edge NEXAFS spectrum. The carbon spectra of different cells are qualitatively similar and display at least five peaks, and likely more, as some peaks may overlap (Fig. 4). Using the reference spectra of Lawrence *et al.* (2003), these peaks can be assigned to different C-containing functional groups. The peaks observed in this study are at the same energy positions as the corresponding peaks measured by Lawrence *et al.* (2003) but show an almost systematic 0.3 eV shift relative to peaks in the same compounds reported in the C K-edge spectral database of Myneni (2002). The first peak at 285.2 eV is likely related to aromatic groups in proteins (Kaznacheyev *et al.*, 2002; Myneni, 2002). The peaks at 286.8 eV and 288.2 eV likely correspond to phenolic groups or ketonic groups or both (Myneni, 2002) and to amide carbonyl groups in proteins, respectively. However, the latter peak is much broader than that observed for albumin, suggesting that the 288.2 eV peak observed for *C. crescentus* corresponds to a combination of both protein amide groups and polysaccharide carboxylic groups. The peak at 289.5 eV is at the same energy position as that of the C = O groups in nucleic acids. Finally, the peak at 290.3 eV was observed only in *C. crescentus* cultured in the calcification medium. This peak is indicative of the presence of carbonate groups.

A C-containing polymeric material bridging between two cells can be seen in Fig. 4C. The C K-edge NEXAFS spectrum from this area shows peaks at 286.9 and 288.5 eV. The latter peak is slightly shifted towards higher energies relative to the main peak observed for the cells and is assigned to carboxylic groups in polysaccharides based on comparison with reference spectra reported by Lawrence *et al.* (2003). This extracellular polymer thus likely corresponds to exopolysaccharides (EPS), which have been shown to be produced by this strain (Ravenscroft *et al.*, 1991). The peak at 286.9 eV, which is assigned to phenolic or ketonic groups, is thus also thought to be related to polysaccharides at least partly. No carbonate peak was observed in this area.

Fig. 4 Spectromicroscopy on *C. crescentus* cells shown in Figs 2 and 3 at the carbon K-edge. (A) STXM image taken at 280 eV, which is below the carbon K-edge. (B) STXM image taken at 288.2 eV (i.e. the resonance energy of amide carbonyl groups in proteins). Dark spots are related to thickness effects. An appendage is observed on the cell in the middle of the picture and was observed for many other cells. (C) Image taken at 288.5 eV (i.e the resonance energy of carboxylic groups in polysaccharides). The polymeric material between the two cells on the right hand side is at maximum visibility at this energy. (D) Carbon K-edge NEXAFS spectra of two *C. crescentus* cells (spectra 1 and 2), and the EPS (spectrum 3) resulting from the image stack on the area depicted in Fig. 4 (A). All the areas are outlined on Fig. 4B. The cell spectra were identical for all the areas tested. Reference spectra of DNA, albumin (taken as a model for protein), and alginate (taken as a model for acidic polysaccharides) are shown for comparison. Labelling of the peaks: a*, aromatic groups at 285.2 eV; k*, ketonic/phenolic groups at 286.8 eV; p*, amide carbonyl group (peptidic bond) at 288.2 eV; cx*, carboxylic groups at 288.5 eV; na*, C = O groups in nucleic acids at 289.5 eV; cn*, carbonate groups at 290.3 eV.
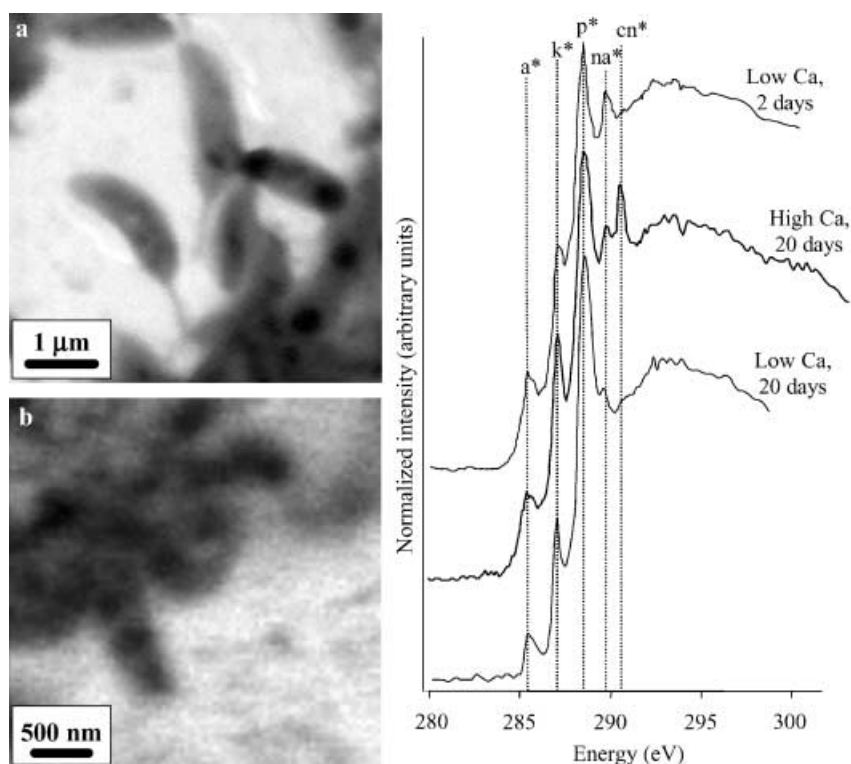
Fig. 5 Spectromicroscopy on *C. crescentus* cells grown in regular PYE medium for (A) 2 days and (B) 20 days. Images were taken at 288.2 eV. Cells grown for 2 days show a well defined kidney bean shape and display appendages similar to those on cells grown for 20 days in the calcification medium. The cells grown for 20 days in the regular PYE growth medium appear degraded. The presence of fragments is suggested because of the electron-dense background. (C) Carbon K-edge NEXAFS spectra of the cells grown under three different conditions: grown for 2 days in regular medium, grown for 20 days in the calcification medium, and grown for 20 days in regular medium. Spectra were identical for different cells in each condition. The carbonate peak at 290.3 eV is unique to the culture grown in the calcium-rich medium. The intensities of the nucleic acid peaks at 289.5 eV for the three samples are significantly different. Peak labelling, Fig. 4 see caption.

C K-edge NEXAFS spectra of *C. crescentus* cultured for two days and 20 days, respectively, in the regular PYE growth medium were measured and compared with the spectrum from *C. crescentus* cells cultured for 20 days in the calcification medium (Fig. 5). Only one spectrum is shown for each condition, but more than 10 spectra showing insignificant variation were measured for each case. The cells cultured in the regular growth medium showed the same features as previously described, with the exception of the carbonate peak at 290.3 eV. Hence, carbonates are associated with phosphorus- and calcium-rich cells.

For the 20 day-old culture grown in the regular PYE growth medium (i.e. at low Ca concentration), the pellet formed after centrifugation was slightly black, in contrast to the 20-day old culture grown in the calcification medium. This suggests that some lysis occurred in the regular PYE growth medium. This suggestion was confirmed by the STXM observations which show that the shapes of the cells are less well defined in the 20 day-old cultures in the regular PYE growth medium (Fig. 5B). Moreover, the 289.5 eV peak, which corresponds to C = O groups in DNA in these cells, is much weaker than that in cells from the 2-day old cultures and is also significantly weaker than that in the cells grown for the same amount of time in the calcification medium.

DISCUSSION

Use of Ca L$_{2,3}$ edges to characterize Ca-containing minerals

Calcium K-edge X-ray absorption spectra are good indicators of calcium coordination environments and hence, provide a convenient means of characterizing even poorly crystalline Ca-containing minerals (e.g. Combes *et al.*, 1991; Sowrey *et al.*, 2004). Although it is not possible to access the K-edge of Ca (4038 eV) on soft-X-ray synchrotron beam lines, it is possible to measure Ca L-edge NEXAFS spectra on such beam lines. However, very few Ca L$_{2,3}$-edge NEXAFS spectra have been reported to date in the geological and geobiological literature (e.g. Doyle *et al.*, 2004). Our study confirms that Ca L$_{2,3}$-edge NEXAFS spectra can be used to distinguish among different Ca-containing minerals important in biomineralization processes.

De Groot *et al.* (1990) and Naftel *et al.* (2001) show that the multipeak pattern of the Ca L$_{2,3}$ edge is the result of the crystal field whose magnitude and symmetry arise from the arrangement of atoms in the first coordination sphere surrounding Ca^{2+}. In addition, because NEXAFS is only sensitive to the local coordination environments of calcium atoms, Ca L$_{2,3}$ NEXAFS spectroscopy is applicable to Ca-containing nanocrystals or poorly crystallized solids, which are common in biomineralized systems (Weiner & Dove, 2003). Calcium in both calcite and vaterite is 6-fold coordinated by oxygen atoms. The spectra for these two CaCO$_3$ polymorphs are very similar in terms of number and energy position of the peaks. However, the intensity ratios for peaks at 348.1 and 349.3 and at 351.4 and 352.6 are very different. Calcium in aragonite is 9-coordinated by oxygen, which explains why the Ca L$_{2,3}$-edge of aragonite is very different from those of calcite and vaterite.

Calcium phosphate precipitation in *Caulobacter crescentus*

The presence of both calcium and phosphorus at equivalent concentrations in *Caulobacter crescentus* cells cultured for 20 days in the PYE growth medium supplemented with calcium suggests that calcium phosphate precipitation occurred in or on the cells. Previous studies have similarly shown the precipitation of calcium phosphate by bacteria when calcium was provided to the growth medium (e.g. Streckfuss *et al.*, 1974; Lucas & Prevot, 1984; Hirschler *et al.*, 1990; Moorer *et al.*, 1993; Ohara *et al.*, 2002). In our study, no calcium phosphate crystal larger than approximately 100 nm was observed outside the cells. Although EPS are usually considered to play an important role in calcium carbonate nucleation in microbialites (e.g. Arp *et al.*, 2003), no calcium enrichment was observed in the EPS between cells here. It is worth noting, however, that sensitivity limits of the STXM method may allow only the detection of calcium-containing precipitates and not of adsorbed calcium. This study, like several previous ones (e.g. Van Dijk *et al.*, 1998; Benzerara *et al.*, 2004), shows that calcium phosphate precipitation occurs on or inside the bacterial cells. The exact location cannot be determined by STXM on whole bacteria and would require additional observations on ultrathin sections. However, hydroxyapatite precipitation inside the periplasm, which has been demonstrated for other Gram-negative bacteria (e.g. Van Dijk *et al.*, 1998 and references therein; Benzerara *et al.*, 2004), is a possibility.

In contrast to the calcium maps, the phosphate map indicates that phosphate localization in the cells is patchy. One possible explanation for this patchy distribution is that calcium is associated with phosphorus only in discrete spots and has another speciation in other locations. However, the many Ca L-edges spectra measured on the cells displayed the same features, showing that calcium has the same speciation consistent with hydroxyapatite throughout the cells. The patchy pattern observed in the phosphorus maps may be artefactual and does not necessarily indicate that phosphorus is only present at discrete spots. Indeed, considering that the phosphorus concentrations measured on the cells are close to the detection limit of the STXM technique, only small variations in phosphorus concentrations could induce this patchy pattern. The precipitate formed in or on *C. crescentus* cells may be amorphous calcium phosphate (ACP). This phase has been proposed to form transiently during the formation of calcium phosphates, and Ca K-edge X-ray absorption spectroscopic data have shown that the short-range structure around calcium in ACP is similar to that of crystalline hydroxyapatite, with a slightly lower Ca coordination number (Taylor *et al.*, 1998). However, the structure of ACP and its significance remain widely debated

(Dorozhkin & Epple, 2002). The observed Ca $L_{2,3}$-edge spectra and the presence of carbonate taken together suggest that the dominant precipitate in *C. crescentus* cells in our samples is carbonate-containing hydroxyapatite, which is the most abundant calcium phosphate biomineral (e.g. Elliott, 2002) and has been reported in previous studies of bacterial calcium phosphate precipitation (e.g. Ohara *et al.*, 2002). The C K-edge does not actually provide information about the structural surroundings of carbonate groups. They could be present in calcium carbonate crystals or in hydroxyapatite. STXM cannot distinguish between carbonate hydroxyapatite and a hydroxyapatite mixed with a very small amount of nanometer-sized calcium carbonates. Only transmission electron microscopy (TEM) would help address that issue.

However, indirect evidence argues against the presence of calcium carbonate in our experiments. For example, the pH of the growth medium (7.1) is low for calcium carbonate precipitation to occur. Moreover, no calcium carbonate was detected at the calcium L-edge and no heterogeneity in carbonate distribution was detected at the carbon K-edge. Therefore, we conclude that no calcium carbonate larger than 25 nanometers is present in or on the bacteria. It is likely, thus, that the carbonate groups detected in this study are incorporated into the hydroxyapatite structure by substitution for phosphate groups and, to a lesser extent, OH-ions, as is usually inferred for hydroxyapatite (Mathew & Takagi, 2001). Although STXM is not able to characterize the crystallinity of the precipitates, it provides permissive evidence for the presence of carbonate groups in the calcium phosphate precipitate which is almost unique at this submicrometer scale. The ability of STXM to characterize the speciation of carbon in mineralized cells provides a good signature for the presence of microorganisms vs. simple macromolecules like proteins or polysaccharides. C K-edge NEXAFS spectra of microorganisms show four or five peaks corresponding to C-containing functional groups in the different biochemical compounds (e.g. proteins, polysaccharides, and nucleic acids) comprising *C. crescentus* cells. Although it may be theoretically possible to design nonmicrobial organic mixtures in the lab displaying such a complex spectrum at the C K-edge, with some doubt regarding the peptide bond signal, we believe that the C K-edge spectrum of bacteria is likely unique relative to abiotic systems. The C K-edge spectrum does not, however, provide any information on the metabolic status of the cells, and whether they are alive or dead has to be assessed by other techniques. After 20 days of incubation in Ca-rich PYE growth medium, the mineralized cells retain that biosignature and can thus be unambiguously recognized. Although we cannot quantify precisely the amount of DNA and proteins remaining in the mineralized cells, the signal associated with these molecules is still high in the calcified cells and shows that more than trace amounts remain.

Previous studies have proposed that proteins are preserved through geological time in dinosaur bones (e.g. Embery *et al.*,

2003), however, little is known about the impact of time, temperature and pressure on the preservation of different biochemical compounds in mineralized cells. The comparison between *C. crescentus* cells grown for 20 days in the calcification medium and nonmineralized cells cultured for the same period in regular PYE growth medium shows that nucleic acids are more abundant in the former. Two possible mechanisms could explain this observation: (a) precipitation of calcium phosphates prevents the degradation of nucleic acids by nucleases released by the lysis of *C. crescentus* cells upon aging of the cultures; and (b) calcium at high concentration is toxic, which results in slower growth, delayed cell starvation, and thus, delayed lysis of the cells. In this study, we observed that *C. crescentus* cells cultured in the calcification medium grew more slowly and were morphologically better preserved than those grown in the regular PYE growth medium. Whereas calcium toxicity has rarely been proposed as a cause for calcium phosphate precipitation, it is interesting to note that several studies, which have presented evidence for precipitation of lead phosphate on or in bacteria, have interpreted this phenomenon as a resistance mechanism to lead toxicity (e.g. Levinson *et al.*, 1996; Templeton *et al.*, 2003).

C. crescentus was used in this study as a model for calcified bacterial cells without any claim that this bacterium is representative of the diversity of prokaryotes. The specific chemical conditions that were used for the calcifying cultures such as those of high concentration of calcium (comparable to the concentration of calcium in modern seawater), and a high availability of phosphorus, may not accurately mimic a wide range of Ca concentrations in natural environments. However, sewage treatment waters, which are rich in phosphate, wherein the microbial mechanisms of phosphate removal are under investigation (Macrae & Smit, 1991), could be good analogues, although the presence of calcified *Caulobacter* sp. cells in such an environment has not been verified.

Advantages and limitations of STXM in geobiology studies

This study aims to experimentally produce calcified microbial cells similar to those suspected to exist in the geological record (Nathan *et al.*, 1993; Baturin *et al.*, 2000), and, using these samples, to test the capabilities of STXM as an analytical tool for inferring the biogenic origin of Ca-containing minerals. It is beyond the scope of this study to address the validity of the chemical signatures for biogenicity, and we direct the reader to Nealson (2001) and Pasteris & Wopenka (2003) and references therein for a more extensive discussion of this topic. We believe, however, that chemical characterization at the submicrometer scale is necessary to infer the biogenicity of natural objects, including fossilized microorganisms.

Like Raman spectroscopy, STXM offers the possibility to characterize both the mineral and the organic components of a sample with minimal sample preparation and without any

prior dehydration, as the measurements are done at ambient temperature and pressure and can even be done in solution. The maximum thickness of a STXM sample allowing imaging and spectroscopy at the C K-edge is about one micron. This constraint could require prior thinning or powdering procedures for geological samples. STXM requires access to a specialized synchrotron radiation beam line (only about half a dozen such beam lines are currently available worldwide), which results in more limited access compared to Raman spectroscopy, but it provides unique capabilities. For example, the ability of STXM to characterize carbon speciation at a spatial resolution of 25 nanometers is particularly well suited for the typical submicrometer-sized, heterogeneous biominerals of interest in geobiology. TEM-based electron energy loss spectroscopy (EELS) can be used to study much smaller features, but it does not provide the spectral resolution that can be achieved by STXM (i.e. approximately 0.1 eV) at least for current TEMs. We have shown that the carbon K-edge at high spectral resolution allows differentiation between various C-containing functional groups. Bacterial cells display a complex spectrum at the carbon K-edge with contributions from aromatic, carboxylic, and peptidic functional groups. When such functional groups are associated and concentrated in an object that has the size and the morphology of a microorganism, this finding may provide permissive evidence for a biogenic origin of terrestrial carbonate or phosphate deposits. Recent results show that cells from bacterial strains as diverse as *Bacillus subtilis*, *Shewanella oneidensis*, and *Caulobacter crescentus* display almost identical carbon K-edge spectra (data not shown). This suggests that the spectra reported in this study may be good signatures for many bacteria and do not provide any phylogenetic information.

The degree of preservation of these molecules in biomineralized cells as a function of time is another issue to be considered in investigations of geological deposits. Pasteris & Wopenka (2003) have discussed the problem of distinguishing abiotic carbonaceous deposits from biogenic kerogens as aging and metamorphism tend to enrich the residues in aromatic compounds and make them look similar spectroscopically. The ability to study carbon speciation at high spatial resolution with STXM may offer the possibility of detecting small areas with remnants of relatively pristine biomolecules. Another approach may come from the use of STXM to detect the presence of other chemical elements like nitrogen, for example, and to determine their speciation. As the absorption of X-rays is measured in transmission using STXM, the sensitivity is not as good as that achieved by high energy X-ray fluorescence measurements as presented by Kemner *et al.* (2004). This limitation of STXM prevents it from detecting elements at very low concentrations. However, soft X-rays provide better spatial resolution than hard X-rays (25 nm vs. 150 nm as discussed in Kemner *et al.*, 2004) and allow one to study light elements like carbon, nitrogen, and oxygen, which are likely required to assess the biogenicity of an object. A combination of both soft and hard X-ray spectromicroscopy approaches is likely the best solution.

Natural samples are usually highly heterogeneous, and the occurrence of fossilized microbes in such samples may be rare, making the detection of traces of life highly challenging. An important advantage offered by STXM is the energy filtered imaging capability. Indeed, it is possible to scan quickly (in a few seconds) relatively large areas (e.g. $40 \, \mu m \times 40 \, \mu m$) of a sample at an energy at which carbon absorbs. By taking the image of the same area below the carbon K-edge, it is then possible to map areas rich in carbon as is shown in Figs 1(C), 2(C) and 3(C). It is possible to be even more specific when looking for microorganisms by taking advantage of the fact that they absorb strongly at an energy characteristic of peptides (288.2 eV). However, other carbon functional groups may absorb a little at this energy. Most of their contribution can be removed by taking an image at a close energy (e.g. 288.6 eV) and subtracting this image from the other.

Although the present study has not proven that a certain class of organic molecule is responsible for the formation of calcium phosphates in *C. crescentus*, it has been able to distinguish among several different biochemical compounds, including proteins, EPS, and DNA associated with hydroxyapatite biominerals in or on these cells. Proteins, polysaccharides, or lipids have been shown experimentally to be potential matrices for the precipitation of calcium-containing minerals (e.g. Bradt *et al.*, 1999; Collier & Messersmith, 2001; Veis, 2003; Zhang *et al.*, 2004), but the relative importance of each class of molecules for calcification in nature is yet to be determined. The study of natural carbonate and phosphate deposits of suspected biogenic origin by STXM may help in determining which of these biomolecules are the most frequent ones associated with calcium carbonates and calcium phosphates in nature. Finally, we suggest that characterization of purported nanobacteria by STXM could help resolve the debate about whether they are calcified microorganisms or calcified macromolecules of a single type, such as proteins.

ACKNOWLEDGEMENTS

DNA, albumin and sodium alginate. The STXM studies were conducted on branch line 11.0.2.2 at the Advanced Light Source, which is supported by the Office of Science, Office of Basic Energy Sciences, Division of Materials Sciences, and Division of Chemical Sciences, Geosciences, and Biosciences of the U.S. Department of Energy at Lawrence Berkeley National Laboratory under contract No. DE-AC03-76SF00098. We thank Kurt Konhauser and three anonymous reviewers for helping to improve this article.

REFERENCES

Arp G, Reimer A, Reitner J (2003) Microbialite formation in seawater of increased alkalinity, Satonda crater lake, Indonesia. *Journal of Sedimentary Research* **73**, 105–127.

Baturin GN, Dubinchuk VT, Zhegallo EA (2000) Bacteria-like formations in phosphorites of the Namibian shelf. *Oceanology* **40**, 737–741.

Benzerara K, Menguy N, Guyot F, Skouri-Panet F, DeLuca G, Barakat M, Heulin H (2004) Biologically controlled precipitation of calcium phosphate by *Ramlibacter tataouinensis*. *Earth Planet Science Letters* **228**, 439–449.

Benzerara K, Yoon TH, Menguy N, Tyliszczak T, Brown GE, JR (2005a) Nanoscale environments associated with bioweathering of a Mg-Fe-Pyroxene. *Proceedings of the National Academy of Sciences of the USA* **102**, 979–982.

Blake RE, Alt JC, Martini AM (2001) Oxygen isotope ratios in PO₄: an inorganic indicator of enzymatic activity and P metabolism and a new biomarker in the search for life. *Proceedings of the National Academy of Sciences of the USA* **98**, 2148–2153.

Bradt JH, Mertig M, Teresiak A, Pompe W (1999) Biomimetic mineralization of collagen by combined fibril assembly and calcium phosphate formation. *Chemistry Mat* **11**, 2694–2701.

Collier JH, Messersmith PB (2001) Phospholipid strategies in biomineralization and biomaterials research. *Annals of Review of Mat Science* **31**, 237–263.

Combes J-M, Brown GE, Jr. Waychunas GA (1991) X-ray absorption study of the local Ca environment in silicate glasses. In *XAFS VI, 6th International Conference on X-Ray Absorption Fine Structure* (ed. Hasnain SS). Ellis Horwood Ltd, Publishers, Chichester, UK pp. 312–314.

De Groot FMF, Fuggle JC, Thole BT, Sawatzky GA (1990) 2p X-ray absorption of 3d transition-metal compounds – an atomic multiplet description including the crystal-field. *Physical Review of B* **42**, 5459–5468.

Dorozhkin SV, Epple M (2002) Biological and medical significance of calcium phosphates. *Ang Chem Intl Ed* **41**, 3130–3146.

Doyle CS, Kendelewicz T, Brown GE Jr (2004) Inhibition of the reduction of Cr (VI) at the magnetite–water interface by calcium carbonate coatings. *Applied Surf Science* **230**, 260–271.

Elliott JC (2002) Calcium phosphate biominerals. *Review of Mineral and Geochemistry* **48**, 427–453.

Embery G, Milner AC, Waddington RJ, Hall RC, Langley MS, Milan AM (2003) Identification of proteinaceous material in the bone of the dinosaur Iguanodon. *Connective Tissue Research* **44**, 41–46.

Folk RL (1999) Nanobacteria and the precipitation of carbonate in unusual environments. *Sedimen Geology* **126**, 47–55.

Ghidoni JJ (2004) Role of *Bartonella henselae* endocarditis in the nucleation of aortic valvular calcification. *Annals of Thoracic Surgery* **77**, 704–706.

Hirschler A, Lucas J, Hubert J-C (1990) Bacterial involvement in apatite genesis. *FEMS Microbiological Ecology* **73**, 211–220.

Hitchcock AP (2000) http://unicorn.mcmaster.ca/aXis2000.html.

Kajander EO, Ciftcioglu N, Aho K, Garcia-Cuerpo E (2003) Characteristics of nanobacteria and their possible role in stone formation. *Urological Research* **31**, 47–54.

Kaznacheyev K, Osanna A, Jacobsen C, Plashkevych O, Vahtras O, Agren H (2002) Inner shell absorption spectroscopy of amino acids. *Journal of Physical Chemistry A* **106**, 3153–3168.

Kemner KM, Kelly SD, Lai B, Maser J, O'Loughlin EJ, Sholto-Douglas D, Cai ZH, Schneegurt MA, Kulpa CF, Nealson KH (2004) Elemental and redox analysis of single bacterial cells by X-ray microbeam analysis. *Science* **306**, 686–687.

Kralj D, Brecevic L, Nielsen AE (1994) Vaterite growth and dissolution in aqueous-solution.2. kinetics of dissolution. *Journal of Cryst Growth* **143**, 269–276.

Lawrence JR, Swerhone GDW, Leppard GG, Araki T, Zhang X, West MM, Hitchcock AP (2003) Scanning transmission X-ray, laser scanning, and transmission electron microscopy mapping of the exopolymeric matrix of microbial biofilms. *Applied Environmental Microbiology* **69**, 5543–5554.

Levinson HS, Mahler I, Blackwelder P, Hood T (1996) Lead resistance and sensitivity in *Staphylococcus aureus*. *FEMS Microbiological Letters* **145**, 421–425.

Lucas J, Prevot L (1984) Apatite synthesis by bacterial activity from phosphatic organic matter and several calcium carbonates in natural fresh-water and seawater. *Chemistry Geology* **42**, 101–118.

Macrae JD, Smit J (1991) Characterization of Caulobacters isolated from waste water treatments. *Applied Environmental Microbiology* **57**, 751–758.

Mathew M, Takagi S (2001) Structures of biological minerals in dental research. *Journal of Research Nat Institute Standards Technology* **106**, 1035–1044.

Miller VM, Rodgers G, Charlesworth JA, Kirkland B, Severson SR, Rasmussen TE, Yagubyan M, Rodgers JC, Cockerill FR, Folk RL, Rzewuska-Lech E, Kumar V, Farell-Baril G, Lieske JC (2004) Evidence of nanobacterial-like structures in calcified human arteries and cardiac valves. *American Journal of Physiological-Heart Circulation Physiology* **287**, H1115–H1124.

Mojzsis SJ, Arrhenius G (1998) Phosphates and carbon on Mars: exobiological implications and sample return considerations. *Journal of Geophysics Research* **103** (E12), 28495–28511.

Moorer WR, Tencate JM, Buijs JF (1993) Calcification of a cariogenic streptococcus and of *Corynebacterium (Bacterionema) Matruchotii* *Journal of Dentistry Research* **72**, 1021–1026.

Myneni SCB (2002) Soft X-ray spectroscopy and spectromicroscopy studies of organic molecules in the environment. *Review of Mineral Geochemistry* **49**, 485–579.

Naftel SJ, Sham TK, Yiu YM, Yates BW (2001) Calcium 1-edge XANES study of some calcium compounds. *Journal of Synchrotron Rad* **8**, 255–257.

Nathan Y, Bremner JM, Lowenthal RE, Monteiro P (1993) Role of bacteria in phosphorite genesis. *Geomicrobiological Journal* **11**, 69–76.

Nealson K (1999) Panel 2: discussion, in size limits of very small microorganisms. Space Studies Board, National Research Council: Washington, DC. National Academy Press, pp. 39–42.

Nealson KH (2001) Searching for life in the universe – lessons from the Earth. *Annals of the New York Academy of Sciences* **950**, 241–258.

Nierman WC, Feldblyum TV, Laub MT, Paulsen IT, Nelson KE, Eisen J, Heidelberg JF, Alley MRK, Ohta N, Maddock JR, Potocka I, Nelson WC, Newton A, Stephens C, Phadke ND, Ely B, DeBoy

RT, Dodson RJ, Durkin AS, Gwinn ML, Haft DH, Kolonay JF, Smit J, Craven MB, Khouri H, Shetty J, Berry K, Utterback T, Tran K, Wolf A, Vamathevan J, Ermolaeva M, White O, Salzberg SL, Venter JC, Shapiro L, Fraser CM (2001) Complete genome sequence of *Caulobacter crescentus*. *Proceedings of the Nat Academy of Sciences of the USA* **98**, 4136–4141.

Ohara N, Ohara N, Yanagiguchi K, Yamada S, Viloria IL, Hayashi Y (2002) Expression of alkaline phosphatase induces rapid and artificial mineralization in specific transformed *Escherichia coli*. *Microbiologica* **25**, 107–110.

Pasteris JD, Wopenka B (2003) Necessary, but not sufficient: Raman identification of disordered carbon as a signature of ancient life. *Astrobiology* **3**, 727–738.

Poindexter JS (1981) The caulobacters – ubiquitous unusual bacteria. *Microbiological Reviews* **45**, 123–179.

Ravenscroft N, Walker SG, Dutton G, Gs Smit J (1991) Identification, isolation and structural studies of extracellular polysaccharides produced by *Caulobacter crescentus*. *Journal of Bact* **173**, 5677–5684.

Rieger D, Himpsel FJ, Karlsson UO, McFeely FR, Morar JF, Yarmoff JA (1986) Electronic-structure of the CAF_2/Si (111) interface. *Physical Review of B* **34**, 7295–7306.

Sanchez-Navas N, Martin-Algarra A (2001) Genesis of apatite in phosphate stromatolites. *European Journal of Miner* **13**, 361–376.

Sowrey FE, Skipper LJ, Pickup DM, Drake KO, Lin Z, Smith ME, Newport RJ (2004) Systematic empirical analysis of calcium-oxygen coordination environment by calcium K-edge XANES. *Physical Chemistry Chemical Physics* **6**, 188–192.

Streckfuss JL, Smith WN, Brown LR, Campbell MM (1974) Calcification of selected strains of *Streptococcus mutans* and *Streptococcus sanguis*. *Journal of Bact* **120**, 502–506.

Taylor MG, Simkiss K, Simmons J, Wu LNY, Wuthier RE (1998) Structural studies of a phosphatidyl serine-amorphous calcium phosphate complex. *Cell Molecular Life Science* **54**, 196–202.

Templeton AS, Trainor TP, Spormann AM, Newville M, Sutton SR, Dohnalkova A, Gorby Y, Brown GE Jr (2003) Sorption vs. biomineralization of Pb (II) within *Burkholderia cepacia* biofilms. *Environmental Science Technology* **37**, 300–307.

Trion A, van der Laarse A (2004) Vascular smooth muscle cells and calcification in atherosclerosis. *American Heart Journal* **147**, 808–814.

Tyliszczak T, Warwick T, Kilcoyne ALD, Fakra S, Shuh DK, Yoon TH, Brown GE, Jr Andrews S, Chembrolu V, Strachan J, Acremann Y (2004) Soft X-ray scanning transmission microscope working in an extended energy range at the advanced light source. *Synchrotron Radiation Instrumentation 2003, AIP Conference Proceedings* **705**, 1356–1359.

Vali H, McKee MD, Çiftçioglu N, Sears SK, Plows FL, Chevet E, Ghiasi P, Plavsic M, Kajander EO, Zare RN (2001) Nanoforms: a new type of protein-associated mineralization. *Geochemica Cosmochemica Acta* **65**, 63–74.

Van Dijk S, Dean DD, Zhao Y, Cirgwin JM, Schwartz Z, Boyan BD (1998) Purification, amino acid sequence, and cDNA sequence of novel calcium-precipitating proteolipids involved in calcification of *Corynebacterium matruchotii*. *Calcif Tissue International* **62**, 350–358.

Veis A (2003) Mineralization in organic matrix frameworks. *Review of Mineral Geochemistry* **54**, 249–289.

Weiner S, Dove PM (2003) An overview of biomineralization processes and the problem of the vital effect. *Review of Mineral Geochemistry* **54**, 1–29.

Yoon TH, Johnson SB, Benzerara K, Doyle CS, Tyliszczak T, Shuh DK, Brown GE Jr (2004) *In situ* characterization of aluminum-containing mineral-microorganism aqueous suspensions using scanning transmission X-ray microscopy. *Langmuir* **20**, 10361–10366.

Zhang LJ, Liu HG, Feng XS, Zhang RJ, Zhang L, Mu YD, Hao JC, Qian DJ, Lou YF (2004) Mineralization mechanism of calcium phosphates under three kinds of Langmuir monolayers. *Langmuir* **20**, 2243–2249.